Article

The Definition of Power Grid Strength and Its Calculation Methods for Power Systems with High Proportion Nonsynchronous-Machine Sources

Zheng Xu * , **Nan Zhang** , **Zheren Zhang and Ying Huang**

Department of Electrical Engineering, Zhejiang University, Hangzhou 310027, China
* Correspondence: xuzheng007@zju.edu.cn

Abstract: This paper studies the definition and calculation method of power grid strength in the environment of high-proportion nonsynchronous-machine sources, focusing on the effect of nonsynchronous-machine sources on voltage support strength and frequency support strength. By dividing the nonsynchronous-machine sources into four types, the equivalent circuits of each type under normal state and fault state are derived, respectively. Based on the Thevenin equivalent impedance of the power grid and the equivalent impedance of the connected device, the definition and calculation method of voltage support strength is given, and the new meaning of single-infeed short-circuit ratio and multi-infeed short-circuit ratio in the context of high proportion nonsynchronous-machine sources is presented. Based on the initial frequency change rate and the steady-state frequency deviation of any node in the power grid under the maximum expected active power disturbance, the equivalent inertia lifting factor and steady-state frequency deviation decreasing factor are defined, respectively, to describe the contribution of nonsynchronous-machine sources to the power grid frequency support strength, and the calculation methods of the equivalent inertia lifting factor and the steady-state frequency deviation decreasing factor are given.

Keywords: power grid strength; voltage stiffness; short-circuit ratio; inertia; frequency change rate; frequency deviation factor

1. Introduction

Power grid strength is one of the fundamental concepts of the power system. It is typically used to quantify the effect of interaction between the grid and the connected device, and the above-mentioned connected device can be a power source, a load, or a station of various types. The most straightforward explanation of power grid strength is the classic concept of an infinite power source. If a bus in the power system is referred to as an infinite power source, it has two connotations [1–3]: The first connotation is that the voltage amplitude of the bus will remain constant regardless of the type and capacity of the connected device, and the second connotation is that the voltage frequency of the bus will remain constant regardless of the type and capacity of the connected device. It can be seen that for the infinite power source, its voltage amplitude and frequency are not affected by the type and capacity of the connected device. For the actual power grid, the voltage amplitude and frequency of any bus must be affected by the type and capacity of the connected device, and the corresponding index describing the degree of effect is the power grid strength. Corresponding to the first connotation of an infinite power source, we use the voltage support strength to describe the degree of voltage amplitude change by the connection of the device, and corresponding to the second connotation of an infinite power source, we use the frequency support strength to describe the degree of voltage frequency change by the connection of the device. Thus, the so-called infinite power source can be understood as the power source with infinite grid strength.

In the traditional power system dominated by synchronous generators, the voltage support strength is usually represented by the short circuit ratio (SCR) [4–6]. The SCR is defined as the ratio of the three-phase short-circuit capacity of the connecting bus (the interface bus between the connected device and the grid, denoted as the point of common coupling (PCC) in the following) to the capacity of the connected device. The three-phase short-circuit capacity here refers to the short-circuit capacity provided by the synchronous generators. In traditional power systems, the typical application of SCR is to describe the power grid strength when the high voltage direct current (HVDC) transmission converter station is connected. It is generally believed that the HVDC transmission converter station can operate stably when SCR is greater than 3 [4–6].

With the transition from a traditional power system to a new type of power system with a high proportion of nonsynchronous-machine sources, it is unreasonable to continue using the conventional SCR definition to describe the voltage support strength. This is because the conventional SCR definition considers only the short-circuit current supplied by the synchronous generators, ignoring the contribution of nonsynchronous-machine sources. Then, a question naturally arises: if the short-circuit current of the nonsynchronous-machine source is considered in the calculation of the SCR, is it still possible to utilize the conventional SCR definition to characterize the voltage support strength? The answer is no, and the reasons for this statement will be presented in later sections of this paper. For the new type of power system, the voltage support strength indexes extended from the conventional SCR definition have been extensively studied. Reference [7] proposes a generalized short circuit ratio (GSCR) based on a modal method to decouple the multi-infeed system. However, the modal method is difficult to calculate, so its engineering applicability is limited. Reference [8] presents a multiple renewable energy station short circuit ratio (MRSCR) based on the ratio of system short circuit capacity to grid-connected capacity of new energy, which has engineering applicability. However, the precision of its calculations is insufficient because only the external properties of new energy as current sources are considered. Therefore, how to define the voltage support strength in the new type of power system considering both accuracy and engineering applicability is a pressing issue that must be tackled [9,10].

In the actual power system, frequency support strength usually exhibits its meaning in two dimensions. The first is the inertia support capability [1–3], which describes the initial frequency change rate after an active power disturbance to the power grid. The second is the primary frequency regulation capability [1–3], which describes the amount of active power that the power grid can absorb or release during the frequency deviation.

In the traditional power system dominated by synchronous generators, the inertia support capability can be expressed by the kinetic energy stored in the rotors of the synchronous generators in the entire grid, and its unit is MWs. It can also be described by the equivalent inertia time constant of the whole grid H. In other words, H is the time required for the kinetic energy stored in the rotors of grid-wide synchronous generators to be released to zero at the constant active power equaling the total capacity of the grid-wide synchronous generators in the unit of second. For the calculation of inertia and the minimum inertia demand, there have been numerous pertinent discussions in the literature [11–22] from the generating unit and system perspectives. In contrast to the synchronous generator, where the inertia is constant, the inertia of the nonsynchronous-machine source is dependent on its control system, and the amount of the inertia varies with the change of the operating point of the nonsynchronous-machine source. Therefore, the total inertia of the system changes with the operation state from the system's perspective. However, how to calculate the inertia support capability in the power system where synchronous generators and nonsynchronous-machine sources coexist is an issue to be solved.

In the traditional power system dominated by synchronous generators, the primary frequency regulation capability is typically described by the frequency deviation factor β [1–3], which is related to the droops of the synchronous generator governors and the frequency sensitivity coefficient of the active load of the whole grid. The unit of β is MW/(0.1 Hz). However, in the power system where synchronous generators and nonsynchronous-machine sources coexist, how to account for the primary frequency regulation capability of the nonsynchronous-machine sources is an urgent problem to be solved.

In this paper, the expressions and the calculation methods of the power grid strength for the power system with high proportion nonsynchronous-machine sources are examined, including the voltage support strength, the inertia support capability, and the primary frequency regulation capability. The rest of the paper is organized as follows. Section 2 discusses the classification and description of the external characteristics of the nonsynchronous-machine sources; Section 3 describes the operating states and their corresponding equivalent circuits for the nonsynchronous-machine sources. Section 4 addresses the definition and calculation method of the voltage support strength at any point in the power grid. Section 5 explores the new meaning of the single-infeed SCR and the multi-infeed SCR. Section 6 addresses the definition and calculation method of the frequency support strength in the power system where synchronous generators and nonsynchronous-machine sources coexist. Finally, Section 7 draws on the conclusion.

2. Classification and Description of the External Characteristics of Nonsynchronous-Machine Sources

The typical structure of nonsynchronous-machine sources is shown in Figure 1 [23]. In Figure 1, U_{dc} and i_{dc} represent the DC voltage and DC current of the voltage source converter (VSC), respectively; u_v and u_s represent the valve-side voltage and the grid-side AC bus voltage of the VSC respectively; P_s and Q_s represent the active power and the reactive power input to the AC grid respectively. On the whole, nonsynchronous-machine sources can be categorized as either grid-forming or grid-following sources [24–31]. The external characteristic of the grid-forming source is an adjustable voltage source, and when its active power is adjustable in a wide range, it can serve as a support source of a passive grid. The external characteristic of the grid-following source is an adjustable current source, and the grid-following source must be connected to the active power grid.
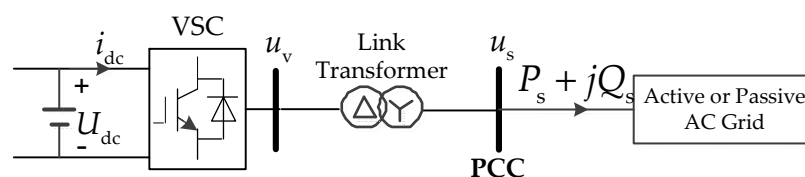
Figure 1. Typical structure of nonsynchronous-machine sources.

2.1. Classification and Controller Structure of Grid-Forming Nonsynchronous-Machine Sources

The grid-forming nonsynchronous-machine sources can be further subdivided into two types according to their active power adjustable capability. The first type is referred to as the Vθ type grid-forming nonsynchronous-machine source, and the second type is referred to as the PV-type grid-forming nonsynchronous-machine source.

2.1.1. Vθ Type Grid-Forming Nonsynchronous-Machine Source

The Vθ type grid-forming nonsynchronous-machine source is characterized by maintaining the amplitude U_{sm} and frequency f of the AC bus voltage at the reference values. For the typical structure of the nonsynchronous-machine sources depicted in Figure 1, the prerequisite for becoming a Vθ type grid-forming nonsynchronous-machine source is that U_{dc} remains essentially constant when the active power output by the VSC to the AC grid varies substantially. Moreover, maintaining a constant U_{dc} is the duty of the external circuit connecting to the DC side of the VSC, not the VSC itself. If the external characteristic of the

Vθ type grid-forming nonsynchronous-machine source is seen from the PCC of the AC grid, it is just analogous to the slack bus in the power flow calculation. In other words, it plays a role in voltage support and power balance in the AC grid. As depicted in Figure 2, the general structure of the controller of the Vθ type grid-forming nonsynchronous-machine source is a three-loop controller. The outermost controller loop is the V/f generator, which determines the reference values of the voltage amplitude U_{sm}^* and frequency f^* of the AC bus voltage us, based on the operating conditions of the DC side of VSC, VSC itself, and the AC grid. The rest dual-loop controller consists of the typical inner and outer loop controllers, where the control principles are mature [32–34] and will not be described here. The inner and outer loop controllers in Figure 2 operate according to U_{sm}^* and the phase angle reference value θ^*; and both the d-axis and q-axis current reference values i_{vd}^* and i_{vq}^* are subjected to the current limiters to prevent the VSC from overcurrent. Besides, u_{vd}^* and u_{vq}^* represent the d-axis and q-axis voltage reference values output by the inner loop current controller, respectively.
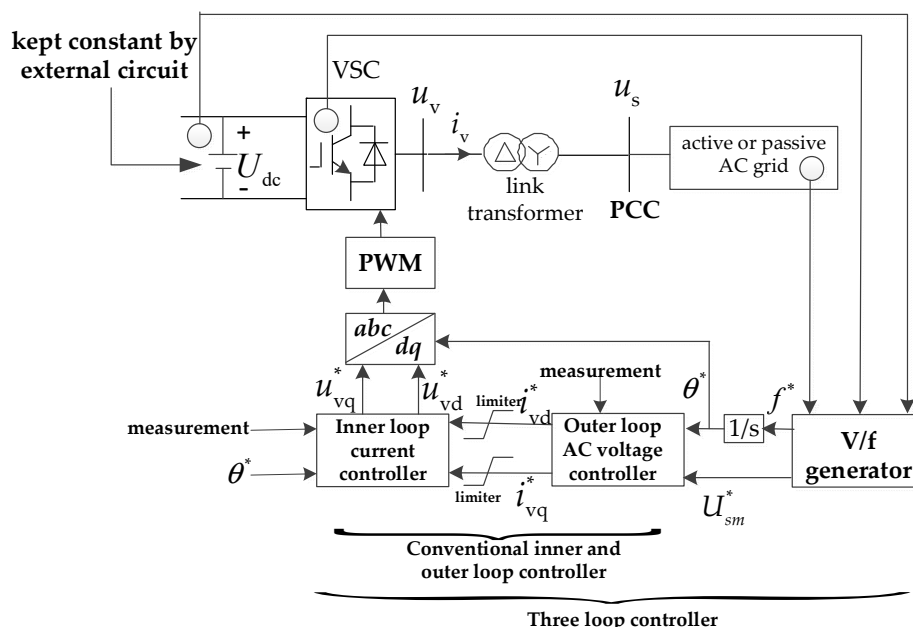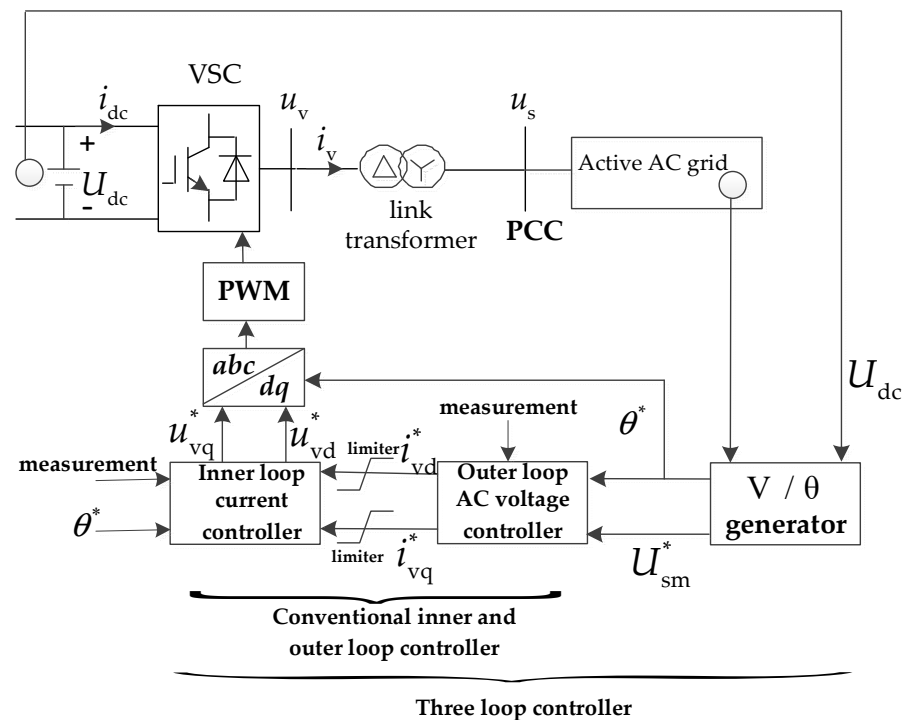

Figure 2. Three-loop controller diagram of the Vθ type grid-forming nonsynchronous-machine source.

2.1.2. PV Type Grid-Forming Nonsynchronous-Machine Sources

The PV-type grid-forming nonsynchronous-machine source is characterized by maintaining U_{sm} at U_{sm}^* and adjusting the phase angle θ to maintain U_{dc} at its reference value U_{dc}^*. The PV-type grid-forming nonsynchronous-machine source corresponds to the photovoltaic units or wind turbines. The following contents use the photovoltaic unit as an illustration of the characteristics of the PV-type grid-forming nonsynchronous-machine source. Assume that the nonsynchronous-machine source shown in Figure 1 is a photovoltaic unit. Under the Maximum Power Point Tracking (MPPT) control condition [35], the reference value U_{dc}^* of U_{dc} is determined by the requirement of the MPPT control; and if the condition of U_{dc} equaling U_{dc}^* is reached, the phase angle θ is set down, and the output active power P_s of VSC is equal to the maximum generating power of the photovoltaic unit. That is, the PV-type grid-forming nonsynchronous-machine source can maintain its AC bus voltage amplitude at its reference value and set down its AC bus voltage phase angle θ according to the value of P_s. However, P_s is changing continuously and equaling the maximum generating power of the photovoltaic unit. Note that the fundamental difference between the PV-type grid-forming nonsynchronous-machine source and Vθ type grid-forming nonsynchronous-machine source is whether it can be used as an independent

support source for the passive power grid. The PV-type grid-forming nonsynchronous-machine source can only operate when connected to the active power grid. If the external characteristic of the PV-type grid-forming nonsynchronous-machine source is seen from the PCC of the AC grid, it is analogous to the PV bus in the power flow calculation. In other words, it supports voltage and outputting determinate active power in the grid. As depicted in Figure 3, the general structure of the controller of the PV-type grid-forming nonsynchronous-machine source is also a three-loop controller. The outermost controller loop is the V/θ generator, which determines θ^* by maintaining U_{dc} at U_{dc}^*, and determines U_{sm}^* based on the operating conditions of the AC grid. The rest dual-loop controller is the same as that in Figure 2.

Figure 3. Three-loop controller diagram of the PV type grid-forming nonsynchronous-machine source.

2.2. Classification and Controller Structure of Grid-Following Nonsynchronous-Machine Sources

According to whether the grid-following nonsynchronous-machine sources are capable of supporting the AC bus voltage, they can be further subdivided into two types: the PV type grid-following nonsynchronous-machine source and the PQ type grid-following nonsynchronous-machine source. The fundamental difference between the grid-following nonsynchronous-machine sources and the grid-forming nonsynchronous-machine sources is whether the phase-locked loop (PLL) is adopted to keep synchronization with the grid [36–41]. Therefore, the grid-following nonsynchronous-machine sources can only operate when connected to the active power grid.

2.2.1. PV Type Grid-Following Nonsynchronous-Machine Sources

The first type of grid-following nonsynchronous-machine source is referred to as the PV type grid-following nonsynchronous-machine source, where the grid synchronization θ is obtained by PLL. The purpose of reactive power control is to maintain U_{sm} at U_{sm}^*, while the objective of active power control is to maintain U_{dc} and P_s at their respective reference values U_{dc}^* and P_s^*. If the external characteristic of the PV-type grid-following nonsynchronous-machine source is seen from the PCC of the AC grid, it is analogous to the PV bus in the power flow calculation. In other words, it plays the role of supporting voltage and outputting determinate active power in the grid. The difference

between the PV-type grid-following nonsynchronous-machine source and the PV-type grid-forming nonsynchronous-machine source is only the control strategy, so the same photovoltaic unit or wind turbine can be constructed as either a PV-type grid-following nonsynchronous-machine source or a PV type grid-forming nonsynchronous-machine source. As depicted in Figure 4, the general structure of the controller of the PV-type grid-following nonsynchronous-machine source is also a three-loop controller. The outermost controller loop is the P/V generator, which determines P_s^* and U_{sm}^* based on the operating conditions of the DC side of the VSC and the AC grid. The rest dual-loop controller consists of the typical inner and outer loop controllers, which are very mature and widely accepted.

Three loop controller
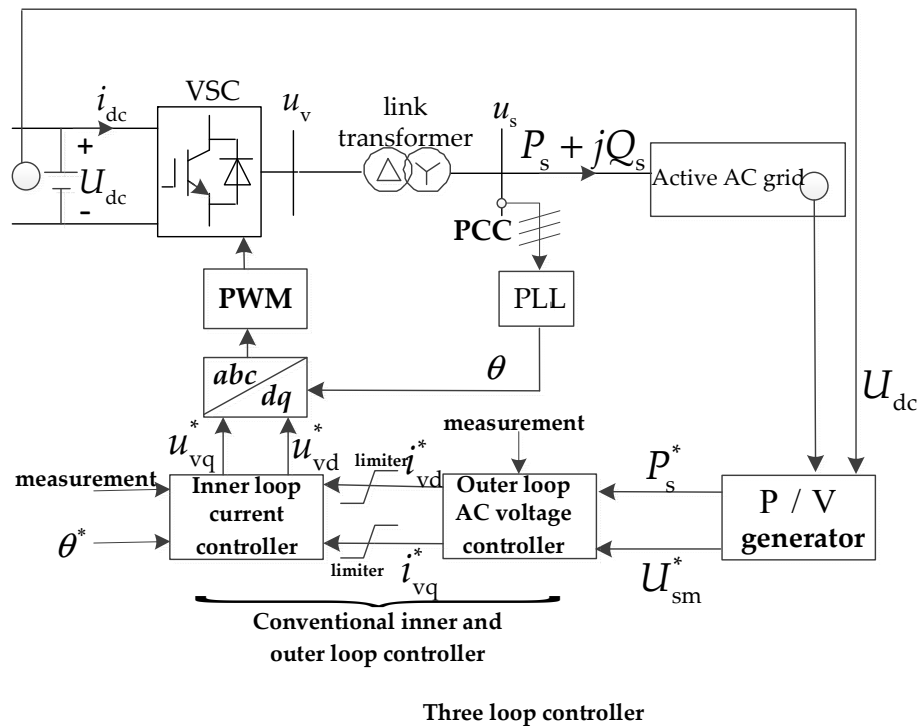
Figure 4. Three-loop controller diagram of the PV type grid-following nonsynchronous-machine source.

2.2.2. PQ Type Grid-Following Nonsynchronous-Machine Sources

The second type of grid-following nonsynchronous-machine source is referred to as the PQ-type grid-following nonsynchronous-machine source, where the control strategy is the same as that of the PV-type grid-following nonsynchronous-machine source. The difference is only in the purpose of the reactive power control. The purpose of the reactive power control of the PQ-type grid-following nonsynchronous-machine source is to maintain the VSC output reactive power Q_s at its reference value Q_s^*. If the external characteristic of the PQ-type grid-following nonsynchronous-machine source is seen from the PCC of the AC grid, it is analogous to the PQ bus in the power flow calculation and injects active and reactive power to the grid. As depicted in Figure 5, the general structure of the controller of the PQ-type grid-following nonsynchronous-machine source is also a three-loop controller. The outermost controller loop is the P/Q generator, which determines P_s^* and Q_s^* based on the operating conditions of the DC side of VSC and the AC grid. The rest dual-loop controller is similar to that in Figure 4.

Figure 5. Three loop controller diagram of the PQ type grid-following nonsynchronous-machine source.

3. Operating State and External Characteristic Equivalent Circuits of Nonsynchronous-Machine Sources

For the four types of nonsynchronous-machine sources described in Section 2, if the three-loop controller shown in Figures 2–5 is used, the outermost loop controller determines the synchronization signal θ^* or the active power reference value (P_s^* or U_{dc}^*) and the reactive power reference value (Q_s^* or U_{sm}^*). The actual control objective is then accomplished by the conventional inner and outer loop controllers, and the final control block adopts the inner loop current controller with direct current control [32–34]. Because of the limiters of i_{vd}^* and i_{vq}^* in the inner loop current controller, once the limiter is activated, the nonsynchronous-machine source enters the current saturation state; and the output of the inner loop current controller can no longer achieve the outer loop controller's predetermined control target. Thus, the external characteristic of the nonsynchronous-machine source depends on whether the inner loop current controller operates in the limiter state. Clearly, the voltage amplitude at the PCC is the primary cause for the inner loop current controller entering the limiter state. Based on the voltage drop range of the PCC, the operating states of the nonsynchronous-machine sources can be classified into two types: the normal state and the fault state. Under the normal state, the voltage of the PCC is close to the rated value, and i_{vd}^* and i_{vq}^* will not exceed the limit values, allowing the nonsynchronous-machine sources to reach the predetermined control target. Under the fault state, the voltage drop of the PCC is relatively large, forcing i_{vd}^* and i_{vq}^* equalling the current limit values. That is, the nonsynchronous-machine source enters the current saturation state and is unable to attain the predetermined control target. The following describes the external characteristic equivalent circuits of the aforementioned four nonsynchronous-machine source types under their normal and fault states.

3.1. External Characteristic Equivalent Circuits of Nonsynchronous-Machine Sources under the Normal State

Under the normal state, a Vθ type grid-forming nonsynchronous-machine source can be equivalent to a voltage source with the constant voltage amplitude and frequency connected to the PCC as viewed from the AC grid.

Under the normal state, a PV-type grid-forming or grid-following nonsynchronous-machine source can be equivalent to a voltage source with the constant voltage amplitude and phase angle connected to the PCC.

Under the normal state, a PQ-type grid-following nonsynchronous-machine source can be equivalent to a current source with a constant current amplitude and phase angle.

3.2. External Characteristic Equivalent Circuits of Nonsynchronous-Machine Sources under the Fault State

Under the fault state, i_{vd}^* and i_{vq}^* equal to the current limit values, the nonsynchronous-machine source enters the current saturation state. Therefore, the nonsynchronous-machine source can be equivalent to a current source with a constant current amplitude and phase angle.

4. Definition and Calculation of Voltage Support Strength at Any Point in the Grid

4.1. Relationship between Thevenin Equivalent Impedance and SCR at Any Bus in the Grid

When exploring the voltage support strength of the power grid, the positive-sequence AC power grid operating at the fundamental frequency is the objective of the investigation. Then, based on the Thevenin equivalence theorem [42,43], when viewed from any bus SYS in the grid, the entire grid can be represented by a Thevenin equivalent circuit, as illustrated in Figure 6. The Thevenin equivalent circuit is composed of the Thevenin equivalent electromotive force $\underline{E}_{th} = E_{th}\angle\theta_{th}$ and the Thevenin equivalent impedance $\underline{Z}_{th} = Z_{th}\angle\varphi_{th}$ connected in series. (Note that this paper represents the complex number with a line at the bottom of the variable). When the device is not connected to the grid, E_{th} equals the no-load voltage at SYS $\underline{U}_{sys0} = U_{sys0}\angle\theta_{sys0}$. $\underline{Z}_{th}$ equals the equivalent impedance when all the independent sources in the fundamental-frequency positive-sequence grid are set to zero, as seen from SYS to the grid.
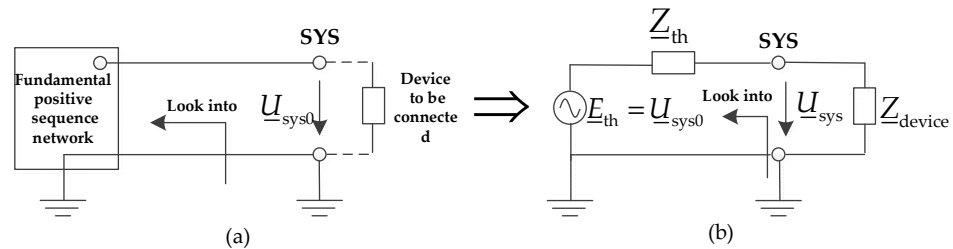

Figure 6. Thevenin equivalence principle of a power grid: (**a**) before the device is connected to the grid; (**b**) after the device is connected to the grid.

The following discussion assumes that when the device is not connected to the grid, the magnitude of the no-load voltage at SYS U_{sys0} is equal to the rated voltage U_N.

Thus, according to Figure 6b, the short-circuit capacity S_{sc} at SYS can be calculated as follows:

$$S_{sc} = \frac{E_{th}^2}{Z_{th}} = \frac{U_{sys0}^2}{Z_{th}} = \frac{U_N^2}{Z_{th}} \tag{1}$$

If the impedance of the connected device is $\underline{Z}_{device} = Z_{device}\angle\varphi_{device}$, the capacity of the connected device at the rated voltage S_{device} is calculated as (2).

$$S_{device} = \frac{U_N^2}{Z_{device}} \tag{2}$$

Then, the short circuit ratio λ_{SCR} of bus SYS corresponding to $\underline{Z}_{device}$ is:

$$\lambda_{SCR} = \frac{S_{sc}}{S_{device}} = \frac{U_N^2}{Z_{th}} \cdot \frac{Z_{device}}{U_N^2} = \frac{Z_{device}}{Z_{th}} \tag{3}$$

Next, we investigate how the device voltage, namely the voltage of bus SYS $\underline{U}_{\text{sys}} = U_{\text{sys}}\angle\theta_{\text{sys}}$, changes after the device is connected to the grid.

According to Figure 6b,

$$
\begin{aligned}
\underline{U}_{\text{sys}} &= \frac{\underline{Z}_{\text{device}}}{\underline{Z}_{\text{device}} + \underline{Z}_{\text{th}}}\underline{U}_{\text{sys0}} \\
&= \frac{\lambda_{\text{SCR}}\angle(\varphi_{\text{device}} - \varphi_{\text{th}})}{1 + \lambda_{\text{SCR}}\angle(\varphi_{\text{device}} - \varphi_{\text{th}})}U_{\text{sys0}}\angle\theta_{\text{sys0}}
\end{aligned}
\tag{4}
$$

According to (4), after the $\underline{Z}_{\text{device}}$ is connected to the grid, the magnitude of the device voltage U_{sys} changes with λ_{SCR}, φ_{device}, and φ_{th}. Considering a typical case, the Thevenin equivalent impedance of the grid is purely inductive, while the equivalent impedance of the connected device is purely resistive, namely, $\varphi_{\text{th}} = 90°$ and $\varphi_{\text{device}} = 0°$, respectively. Under such circumstances, the expression of U_{sys} can be simplified to (5).

$$
U_{\text{sys}} = \frac{\lambda_{\text{SCR}}}{\sqrt{1 + \lambda_{\text{SCR}}^2}}U_{\text{sys0}} = \frac{\lambda_{\text{SCR}}}{\sqrt{1 + \lambda_{\text{SCR}}^2}}U_{\text{N}}
\tag{5}
$$

Based on (5), if $\lambda_{\text{SCR}} \gg 1$, $U_{\text{sys}} \approx U_{\text{N}}$. Otherwise, U_{sys} is always less than U_{N}. The variation characteristic of U_{sys} with λ_{SCR} is shown in Figure 7. When $\lambda_{\text{SCR}} = 5$, $U_{\text{sys}} = 0.98U_{\text{N}}$; when $\lambda_{\text{SCR}} = 3$, $U_{\text{sys}} = 0.95U_{\text{N}}$; and when $\lambda_{\text{SCR}} = 1$, $U_{\text{sys}} = 0.71U_{\text{N}}$. Consequently, it is commonly believed that when SCR is larger than 3, then SYS is a strong bus, as the voltage drop after being loaded is less than 5% of the rated voltage.
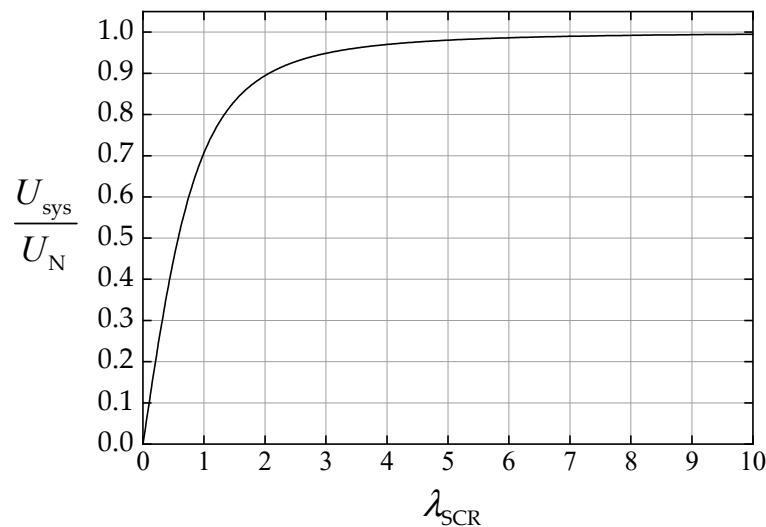
Figure 7. Variation of device voltage with the short-circuit ratio.

4.2. Definition of Voltage Support Strength of Any Bus in the Grid

Inspired by the concept of infinite power source, the voltage support strength of any bus in the grid is defined as the ability to maintain the voltage magnitude close to the no-load voltage. It is described by $U_{\text{sys}}/U_{\text{sys0}}$, which is called the voltage stiffness K_{vtg}. Then according to (4),

$$
\begin{aligned}
K_{\text{vtg}} &= \frac{U_{\text{sys}}}{U_{\text{sys0}}} = \left|\frac{\underline{Z}_{\text{device}}}{\underline{Z}_{\text{th}} + \underline{Z}_{\text{device}}}\right| \\
&= \left|\frac{\lambda_{\text{SCR}}\angle(\varphi_{\text{device}} - \varphi_{\text{th}})}{1 + \lambda_{\text{SCR}}\angle(\varphi_{\text{device}} - \varphi_{\text{th}})}\right|
\end{aligned}
\tag{6}
$$

Obviously, the range of K_{vtg} is [0, 1]. When Z_{th} is zero, K_{vtg} is equal to 1; and when Z_{th} is infinity, K_{vtg} equals zero.

Comparing K_{vtg} to λ_{SCR}, K_{vtg} provides more grid information than λ_{SCR}. λ_{SCR} reflects only the magnitude of $\underline{Z}_{\text{th}}$ and $\underline{Z}_{\text{device}}$, but not their phase angles. In addition, the range

of λ_{SCR} is $[0, \infty]$, while the range of K_{vtg} is $[0, 1]$. Figure 7 can also be regarded as the relationship between short circuit ratio and voltage stiffness under a specific condition.

4.3. Definition of Voltage Support Strength of Any Bus in the Grid

According to (6), K_{vtg} is uniquely determined by $\underline{Z}_{\mathrm{th}}$ and $\underline{Z}_{\mathrm{device}}$. Due to the known impedance of the connected device $\underline{Z}_{\mathrm{device}}$, the calculation of K_{vtg} is equivalent to the calculation of $\underline{Z}_{\mathrm{th}}$.

The external characteristic equivalent circuit of a nonsynchronous-machine source is closely related to its operating states, as determined by the analysis in Section 2. Consequently, the calculation of $\underline{Z}_{\mathrm{th}}$ at any bus in the grid is closely related to the operating states of the nonsynchronous-machine source. Therefore, each nonsynchronous-machine source must be calculated by the equivalent circuit under the corresponding state.

In accordance with the calculation principle of the Thevenin equivalence impedance $\underline{Z}_{\mathrm{th}}$, each independent source in the fundamental-frequency positive-sequence grid is set to zero. This indicates that a branch represents the voltage source is replaced with a short circuit to the ground, and the current source is represented by a branch with an open circuit to the ground. Thus, when calculating $\underline{Z}_{\mathrm{th}}$, the synchronous generator is represented by the impedance branch to ground, and the impedance value is typically set to the transient reactance. However, the branch adopted by the nonsynchronous-machine source depends on its operating states.

When the nonsynchronous-machine sources are under the normal states, the Vθ type grid-forming nonsynchronous-machine source, the PV type grid-forming nonsynchronous-machine source, and the PV type grid-following nonsynchronous-machine source can be represented by branches with short circuits to the ground at their PCCs. In contrast, the PQ-type grid-following nonsynchronous-machine source is represented by the branch with an open circuit to ground at the PCC. When the nonsynchronous-machine sources are under the fault states, all four types are represented by branches with open circuits to ground at their PCCs.

During the actual calculation, due to different fault locations, the voltage drop degree of each bus in the power grid is different. This indicates that for the same fault, the operating state of the different nonsynchronous-machine sources may be different, with some under the fault states and others under the normal states. Therefore, $\underline{Z}_{\mathrm{th}}$ changes with different fault locations in principle. To simplify the analysis, two types of equivalent impedance are defined for any bus in the grid, which is of great significance. The first is called the normal-state Thevenin equivalent impedance $\underline{Z}_{\mathrm{th,nom}}$, and the second is called the fault-state Thevenin equivalent impedance $\underline{Z}_{\mathrm{th,flt}}$. Thus, when calculating $\underline{Z}_{\mathrm{th,nom}}$, it is assumed that all the nonsynchronous-machine sources are under normal states. When calculating $\underline{Z}_{\mathrm{th,flt}}$, it is considered that all the nonsynchronous-machine sources are under the fault states.

In addition, it must be pointed out that when the grid-forming nonsynchronous-machine source does not adopt the conventional inner and outer loop controllers as shown in Figures 2 and 3 but instead adopts the amplitude-phase angle controller without the current inner loop control [44–46], the equivalent circuit of the nonsynchronous-machine source under the fault state is roughly equivalent to the internal electromotive force in series with the total current limiting impedance. The total current limiting impedance is composed of the connected reactance and the virtual impedance, where the value is determined by the controller structure of the nonsynchronous-machine source. The objective of current limiting impedance is to prevent the output current of the nonsynchronous-machine source from exceeding its overload current level under the fault state, which is typically 1.1 times the rated current. Under such circumstances, the fault-state equivalent impedance of the nonsynchronous-machine source is equal to the total current limiting impedance.

4.4. Examples of Calculation of Voltage Stiffness and Short-Circuit Ratio

For the system with renewable energy and static synchronous compensator (STATCOM), as shown in Figure 8 [47], it is assumed that both wind turbines and photovoltaic units adopt grid-following control. The impedance of the transmission line x_{Line} is 40 Ω, and its length is 100 km. The leakage reactance of the transformer u_{k} is 10%, its ratio is 220 kV/500 kV, and its capacity is 300 MVA. x_{T} represents the reactance of the transformer. The transient reactance of the synchronous generator x'_{d} is 10 Ω. The whole output active power of renewable energy is 200 MW. Next, the voltage stiffness and short-circuit ratios are calculated in the following when STATCOM is controlled by the constant AC voltage amplitude control and the constant reactive power control, respectively.
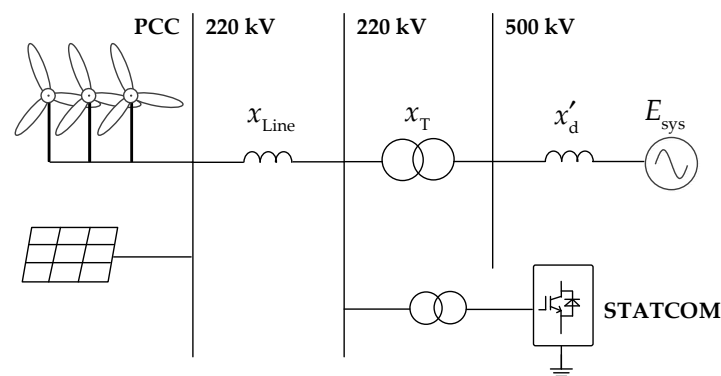
Figure 8. Schematic diagram of the system with new energy sources and STATCOM.

When the STATCOM adopts the constant AC voltage amplitude control and the constant active power control, it is a PV-type grid-following nonsynchronous-machine source. According to the rules stated in Section 3.1, the system's Thevenin equivalent circuits are depicted in Figure 9. For the PCC, the wind turbines and the photovoltaic units are collectively regarded as connected devices. Firstly, the voltage stiffness and short circuit ratio of the PCC are calculated when the STATCOM is in the normal state. The equivalent circuit of the STATCOM is a constant voltage source. The independent voltage source is represented by the branch with a short circuit to the ground when calculating the Thevenin equivalent impedance. Therefore, as shown in Figure 9a, $Z_{\mathrm{th,nom}} = x_{\mathrm{Line}}$ when seen from the PCC to the AC system. Thus, K_{vtg} at the PCC is 0.858, whereas λ_{SCR} at the PCC is 6.05.
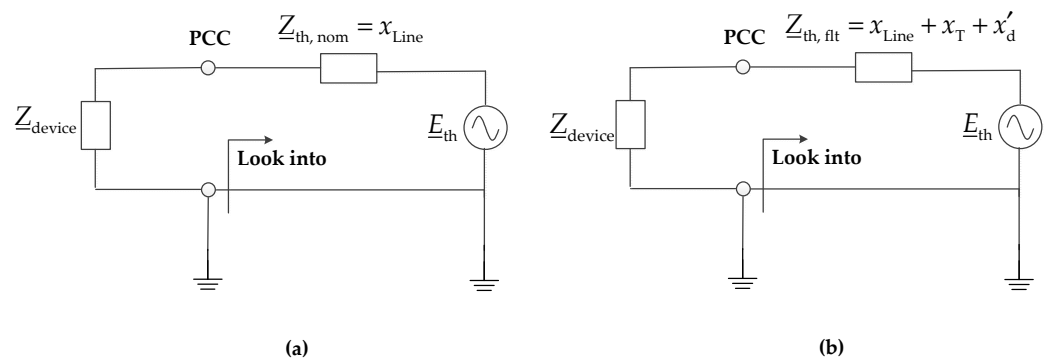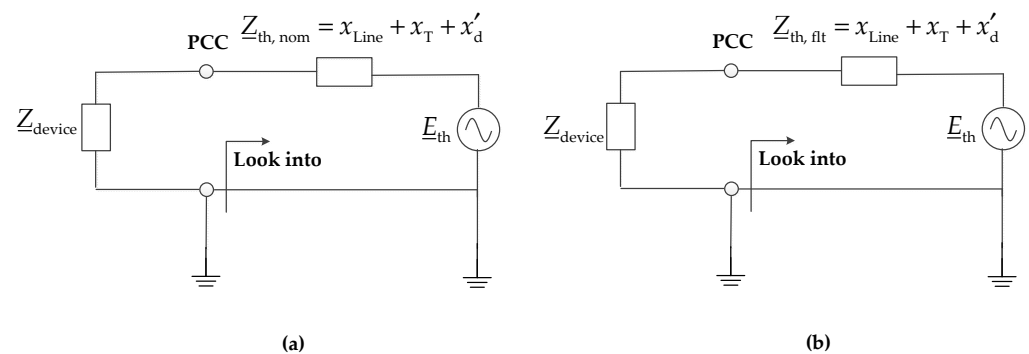

(a)   (b)

Figure 9. Thevenin equivalent circuit of the system when STATCOM adopts the constant AC voltage amplitude control and the constant active power control: (**a**) STATCOM is under the normal state; (**b**) STATCOM is under the fault state.

Then, the voltage stiffness and short-circuit ratio of the PCC are calculated when an AC fault occurs at the 500 kV network, which leads to a large drop in the E_{sys}, and we assume that the AC fault does not change x'_{d}. At this time, due to the AC voltage drop, the STATCOM is under the fault state and operates under the current saturation state. The equivalent

circuit of the STATCOM is a constant current source. When calculating the Thevenin equivalent impedance, the independent current source is represented by the branch with an open circuit to the ground. Therefore, as shown in Figure 9b, $\underline{Z}_{\text{th, flt}} = x_{\text{Line}} + x_{\text{T}} + x'_{\text{d}}$. Therefore, K_{vtg} at the PCC is 0.806, whereas λ_{SCR} at the PCC is 4.167.

When the STATCOM adopts the constant reactive power control and the constant active power control, the system's Thevenin equivalent circuits are depicted in Figure 10. In both scenarios, the equivalent circuit of the STATCOM is a constant current source. When calculating the Thevenin equivalent impedance, the independent current source is represented by the branch with an open circuit to the ground. Therefore, as shown in Figure 10a,b, $Z_{\text{th,nom}} = \underline{Z}_{\text{th, flt}} = x_{\text{Line}} + x_{\text{T}} + x'_{\text{d}}$. Therefore, K_{vtg} at the PCC is 0.806, whereas λ_{SCR} at the PCC is 4.167.

Figure 10. Thevenin equivalent circuit of the system when STATCOM adopts the constant reactive power control and the constant active power control: (**a**) STATCOM is under the normal state; (**b**) STATCOM is under the fault state.

5. New Exploration of Single infeed SCR and Multi-Infeed SCR

The concept of short circuit ratio has been used in the early development stage of HVDC transmission. In 1992 and 1997, the CIGRE working group on AC/DC interaction and the IEEE working group on the interaction between DC transmission systems and AC systems with low SCR jointly published research reports [4–6] and provided a comprehensive and in-depth description of SCR, which has led to its widespread recognition and application in the field of HVDC transmission [48–52].

The concept of single-infeed SCR proposed by CIGRE and IEEE joint Working Group in 1992 was defined based on the short circuit capacity [4]. When there are only synchronous generators in the power grid, the SCR defined based on short circuit capacity is completely consistent with the SCR defined by the Thevenin equivalent impedance, as the short circuit current of the synchronous generator is entirely determined by its impedance, without any current limiters. However, the SCR based on the short circuit capacity definition and the SCR based on the Thevenin equivalent impedance definition is fundamentally different for the nonsynchronous-machine source. Due to overcurrent limiters, it is useless to describe SCR with the short circuit capacity for nonsynchronous-machine sources. In other words, for nonsynchronous-machine sources, the short circuit capacity cannot characterize the ability of a bus to maintain its loaded voltage close to its no-load voltage. When nonsynchronous-machine sources exist, it is more appropriate to define the SCR by the following expression.

$$\lambda_{\text{SCR}} = \frac{Z_{\text{device}}}{Z_{\text{th}}} \qquad (7)$$

Due to the uniform treatment of the synchronous generators and the nonsynchronous-machine sources in this definition, the application of the SCR can be extended to the power grid where synchronous generators and nonsynchronous-machine sources coexist.

In 2007, the CIGRE multiple DC infeed working group [53,54] introduced the notion of effective short circuit ratio (ESCR) to describe the voltage support strength of multiple DC infeed systems. Here we will give a new exploration of the voltage support strength

of multiple DC infeed AC systems. The following example of the double DC infeed AC system demonstrates the new exploration.

The investigated double DC infeed AC system is shown in Figure 11a. In accordance with the Thevenin equivalence concept of the two-port network [55], Figure 11b depicts the equivalent circuit of the double DC infeed AC system. In Figure 9, the infeed bus of the double DC lines is represented by *i* and *j*, respectively, and $\underline{U}_{i\text{o}}$ and $\underline{U}_{j\text{o}}$ represent the voltage phasors (i.e., no-load voltages) when the double DC lines are not connected to the power grid. $\underline{Z}_{ii}$, $\underline{Z}_{jj}$, and $\underline{Z}_{ij}$ are the equivalent impedances of the two-port Thevenin equivalent circuit for the fundamental-frequency positive-sequence AC grid. $\underline{Z}_{\text{DC}i}$ and $\underline{Z}_{\text{DC}j}$ are the equivalent impedances of the double DC lines in their rated operating states.
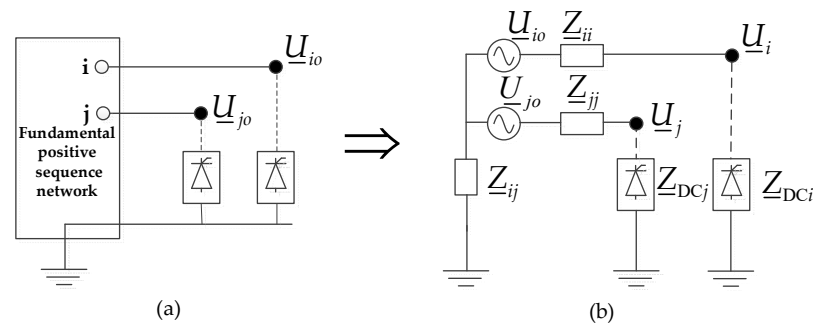
Figure 11. Schematic diagram of a double DC infeed system: (**a**) the original structure of the double DC infeed system; (**b**) the Thevenin equivalent circuit of the double DC infeed system.

Consider the DC line *i* as an example. Firstly, the Thevenin equivalent electromotive force $\underline{E}_{\text{th}}$ and the Thevenin equivalent impedance $\underline{Z}_{\text{th}}$, seen from bus *i* to the grid when DC line *j* is not connected, are studied. Then the Thevenin equivalent electromotive force $\underline{E}_{\text{th}}^{\text{m}}$ and the Thevenin equivalent impedance $\underline{Z}_{\text{th}}^{\text{m}}$ are examined when the DC line *j* is connected to the grid. The superscript "m" here represents the multiple DC infeed.

In the single DC infeed condition, that is, when the DC line *j* is not connected, the $\underline{Z}_{\text{DC}j}$ branch in Figure 9b is an open circuit, and $\underline{E}_{\text{th}}$ and $\underline{Z}_{\text{th}}$ are calculated as (8).

$$\begin{cases} \underline{E}_{\text{th}} = \underline{U}_{io} \\ \underline{Z}_{\text{th}} = \underline{Z}_{ij} + \underline{Z}_{ii} \end{cases} \tag{8}$$

In the multiple DC infeed condition, that is, when DC line *j* is connected, $\underline{E}_{\text{th}}^{\text{m}}$ and $\underline{Z}_{\text{th}}^{\text{m}}$ are calculated as (9).

$$\begin{cases} \underline{E}_{\text{th}}^{m} = \underline{U}_{io}^{m} = \underline{U}_{io} + \frac{\underline{Z}_{ij}}{\underline{Z}_{ij} + \underline{Z}_{jj} + \underline{Z}_{\text{DC}j}} \underline{U}_{jo} \\ \underline{Z}_{\text{th}}^{m} = \underline{Z}_{ii} + \frac{\underline{Z}_{ij}(\underline{Z}_{jj} + \underline{Z}_{\text{DC}j})}{\underline{Z}_{ij} + \underline{Z}_{jj} + \underline{Z}_{\text{DC}j}} \end{cases} \tag{9}$$

The ratios of the Thevenin equivalent electromotive forces and the Thevenin equivalent impedances in the two conditions are shown in (10).

$$\begin{cases} \dfrac{\underline{E}_{\text{th}}^{m}}{\underline{E}_{\text{th}}} = \dfrac{\underline{U}_{io}^{m}}{\underline{U}_{io}} = 1 + \dfrac{\underline{Z}_{ij}}{\underline{Z}_{ij} + \underline{Z}_{jj} + \underline{Z}_{\text{DC}j}} \cdot \dfrac{\underline{U}_{jo}}{\underline{U}_{io}} \\ \dfrac{\underline{Z}_{\text{th}}^{m}}{\underline{Z}_{\text{th}}} = \dfrac{\underline{Z}_{ii}}{\underline{Z}_{ij} + \underline{Z}_{ii}} + \dfrac{\underline{Z}_{ij}}{\underline{Z}_{ij} + \underline{Z}_{ii}} \cdot \dfrac{\underline{Z}_{jj} + \underline{Z}_{\text{DC}j}}{\underline{Z}_{ij} + \underline{Z}_{jj} + \underline{Z}_{\text{DC}j}} \end{cases} \tag{10}$$

For the actual power grid parameters and operating states, the Thevenin equivalent electromotive force changes greatly in the two conditions, while the Thevenin equivalent impedance changes only slightly. Usually,

$$R_{\text{eth}}^{\text{m}} = \frac{E_{\text{th}}^{\text{m}}}{E_{\text{th}}} = \frac{U_{io}^{\text{m}}}{U_{io}} = \left| 1 + \frac{\underline{Z}_{ij}}{\underline{Z}_{ij} + \underline{Z}_{jj} + \underline{Z}_{\text{DC}j}} \cdot \frac{\underline{U}_{jo}}{\underline{U}_{io}} \right| \leq 1 \tag{11}$$

$$R_{zth}^{m} = \frac{\underline{Z}_{th}^{m}}{\underline{Z}_{th}} = \frac{\underline{Z}_{ii}}{\underline{Z}_{ij} + \underline{Z}_{ii}} + \frac{\underline{Z}_{ij}}{\underline{Z}_{ij} + \underline{Z}_{ii}} \cdot \frac{\underline{Z}_{jj} + \underline{Z}_{DCj}}{\underline{Z}_{ij} + \underline{Z}_{jj} + \underline{Z}_{DCj}} \approx 1 \tag{12}$$

$$\lambda_{SCR}^{m} = \frac{Z_{DCi}}{Z_{th}^{m}} \approx \frac{Z_{DCi}}{Z_{th}} = \lambda_{SCR} \tag{13}$$

$$K_{vtg}^{m} = \frac{U_i^m}{U_{io}} = \frac{1}{U_{io}} \left| \frac{\underline{E}_{th}^m \cdot \underline{Z}_{DCi}}{\underline{Z}_{th}^m + \underline{Z}_{DCi}} \right| \approx \frac{E_{th}^m}{U_{io}} \cdot \left| \frac{\underline{Z}_{DCi}}{\underline{Z}_{th} + \underline{Z}_{DCi}} \right| = R_{eth}^m K_{vtg} \tag{14}$$

in (11)–(14), R_{eth}^{m} is the ratio of the Thevenin equivalent electromotive forces seen from bus i to the AC grid in the multiple DC infeed condition and in the single DC infeed condition, which is called the multiple DC infeed no-load voltage drop factor. $\underline{U}_{io}$ is the no-load voltage phasor of bus i in the single DC infeed condition and $\underline{U}_{io}^{m}$ is the no-load voltage phasor of bus i in the multiple DC infeed condition. R_{zth}^{m} is the ratio of the Thevenin equivalent impedances seen from bus i to the AC grid in the multiple DC infeed condition and the single DC infeed condition. λ_{SCR} is the SCR of DC line i in the single DC infeed condition and λ_{SCR}^{m} is the SCR of DC line i in the multiple DC infeed condition. K_{vtg} is the voltage stiffness of DC line i in the single DC infeed condition and K_{vtg}^{m} is the voltage stiffness of DC line i in the multiple DC infeed condition.

As shown in (13), it is insufficient to use the SCR index to characterize the voltage support strength in the multiple DC infeed condition because the values of SCR in single and multiple DC infeed conditions change slightly. However, it is of greater index significance to use voltage stiffness to characterize the voltage support strength in the multiple DC infeed condition because K_{vtg}^{m} can reflect the change in the Thevenin equivalent electromotive force in the multiple DC infeed condition and K_{vtg}^{m} is equal to K_{vtg} multiplied by R_{eth}^{m} in the multiple DC infeed condition.

It is meaningful to compare K_{vtg}^{m} with the multiple DC infeed ESCR proposed by the CIGRE working group [53,54]. It can be found that the multiple DC infeed ESCR cannot directly reflect the drop in the no-load voltage due to multiple DC infeed and does not convey the physical substance of the reduction in voltage support strength in the multiple DC infeed scenario. ESCR, as a voltage support strength index, is difficult to create a unified numerical criterion in practice.

If the DC infeed shown in Figure 9 is generalized by a PQ-type grid-following nonsynchronous-machine source, such as a conventional PQ-type grid-following wind farm or photovoltaic station, the voltage support strength of the AC power grid can also use K_{vtg}^{m} as an index.

6. Definition and Calculation Method of Frequency Support Strength in the New Type Power System

The frequency support strength has two manifestations: the inertia support capability and the primary frequency regulation capability. The synchronous generator has both inertia support capability and primary frequency regulation capability. The inertia of the synchronous generator is independent of its operating point and is a constant value [1–3]. The primary frequency regulation capability of the synchronous generator is closely related to its operating point and the droop of its governor. The load possesses a small amount of inertia support and frequency regulation effect. Different from the synchronous generator, the inertia support capability and primary frequency regulation capability of the nonsynchronous-machine source are entirely determined by its control modes and output power margin. The nonsynchronous-machine source in the early stage is usually controlled by MPPT, and its output power is decoupled from the frequency of the power grid. Under such circumstances, the nonsynchronous-machine source has no support for the frequency stability of the power grid. With the increasing proportion of the nonsynchronous-machine source, the control strategy of the nonsynchronous-machine source must be changed to couple its output power with the grid frequency so as to have inertia support capability and primary frequency regulation capability.

The inertia support and primary frequency regulation capabilities of the power grid can be characterized by the dynamic response curve after a large disturbance [56,57], as shown in Figure 12, in which the actual frequency dynamic response curve is represented by segmented polylines. Line Section 1 represents the inertia response period, while line Sections 2 and 3 represent the inertia response and primary frequency regulation joint action period. Line Section 4 represents the primary frequency regulation period. Based on the frequency dynamic response curve, three parameters are usually used to describe the inertia support and the primary frequency regulation capability of the power grid. The first parameter is the initial rate of change of frequency (RoCoF) of a disturbance, namely the slope of the line Section 1. The second parameter is the highest or lowest frequency, denoted by f_{zenith} or f_{nadir}, respectively. The third parameter is the steady-state frequency deviation, denoted by Δf_{∞}.
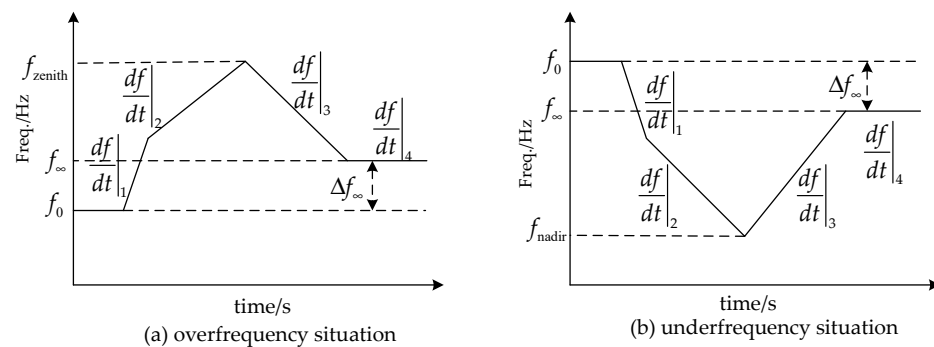
Figure 12. Frequency dynamic response curve describing inertia support and primary frequency regulation capability: (**a**) in the overfrequency situation; (**b**) in the underfrequency situation.

6.1. Implementation of Inertia and Primary Frequency Regulation of Nonsynchronous-Machine Sources

For the Vθ type grid-forming nonsynchronous-machine source shown in Figure 2, it is the support source of the connected grid. Within the range of its current capacity, the grid frequency is entirely determined by it and is unaffected by various grid disturbances. Therefore, in the range of its current capacity, the inertia support provided by the Vθ type grid-forming nonsynchronous-machine source is infinite. However, once it hits the current limit as a result of the fault, the inertia support and primary frequency regulation capabilities are no longer available.

For the PV-type grid-forming nonsynchronous-machine source shown in Figure 3, the inertia support capability is determined by the outermost loop controller, namely the V/θ generator, which usually adopts power synchronization control [57,58] or virtual synchronous machine control [59–66]. It has been proved that power synchronization control and virtual synchronous machine control are essentially consistent [67–69]; hence, the distinction between the two is ignored in this article. After adopting the power synchronization control, the V/θ generator is implemented in accordance with the Vθ decoupling mode. The θ generator is the so-called power synchronization loop (PSL) [57,58], which imitates the swing equation of the synchronous generator. The V generator is usually implemented by a reactive power-voltage droop controller [34].

The principle of PSL is to mimic the nonsynchronous-machine source as a synchronous generator, and the output of PSL is the rotor angle θ [34]. The swing equations of a synchronous generator are:

$$2H\frac{\mathrm{d}\Delta\omega}{\mathrm{d}t} = P_{\mathrm{m}} - P_{\mathrm{e}} - D\Delta\omega \tag{15}$$

$$\frac{\mathrm{d}\theta}{\mathrm{d}t} = \omega \cdot \omega_0 \tag{16}$$

where H is the inertia time constant of the generator (unit: s), which determines the inertia support capability of the nonsynchronous-machine source. $\Delta\omega = \omega_0 - \omega$ is the generator speed deviation. ω is the actual speed (per unit value), and ω_0 is the rated speed (per unit value). t represents the time, where the unit is s. P_{m} and P_{e} are the mechanical power and electromagnetic power (in per unit value); D is the damping coefficient (in per unit value); θ is the generator's electrical rotor angle, where the unit is rad. By substituting the P_{m} of the generator for the active power reference value P_{s}^* of the nonsynchronous-machine source and P_{e} of the generator for the actual active power, P_{s}, of the nonsynchronous-machine source, the control block diagram of PSL is illustrated in Figure 13 [34].
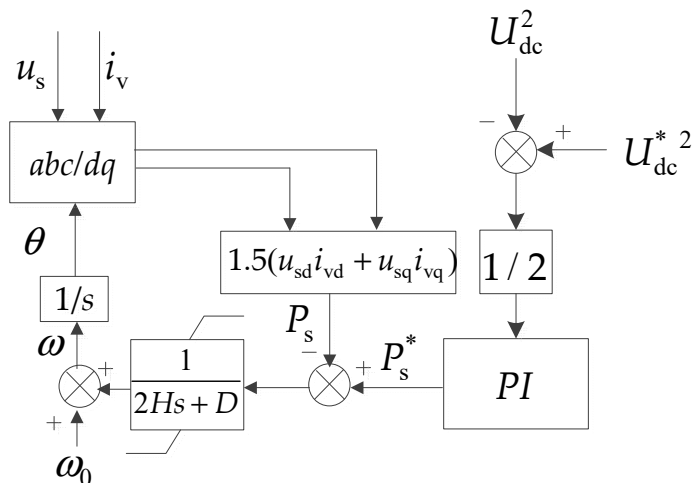
Figure 13. Power synchronization loop diagram of the PV-type grid-forming nonsynchronous-machine source.

Notably, the PV-type grid-forming nonsynchronous-machine source achieves its primary frequency regulation by changing the reference value of the DC voltage U_{dc}^*. It must have the ability to reduce power for frequency regulation but not necessarily have the ability to increase power for frequency regulation. For example, the initial value of U_{dc}^* corresponds to the maximum power output, but the frequency of the grid is too high, so the active power output must be decreased. Consequently, the primary frequency regulation is to make the nonsynchronous-machine source run away from the maximum power point by changing the value of the U_{dc}^* so as to reduce the active output. Conversely, power increase frequency regulation depends on whether the nonsynchronous-machine source has sufficient power support.

The V generator usually adopts the reactive power-voltage droop control [34], and its typical control strategy is shown as (17).

$$U_{\mathrm{sm}}^* = U_{\mathrm{sm0}}^* + k_{\mathrm{p}}(Q_{\mathrm{s}}^* - Q_{\mathrm{s}}) \tag{17}$$

where U_{sm}^* is the reference value of the output voltage; U_{sm0}^* is the base voltage; Q_{s}^* is the reference value of the reactive power; Q_{s} is the actual reactive power. Then, the diagram of the V generator can be obtained in Figure 14.
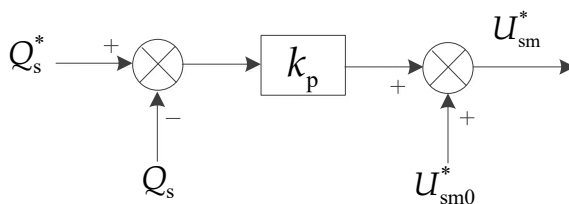

Figure 14. The V generator block diagram of the PV-type grid-forming nonsynchronous-machine source.

For the PV-type grid-following nonsynchronous-machine source in Figure 4, its inertia support and primary frequency regulation capabilities are determined by the outermost loop P/V generator. Still, the premise is that the nonsynchronous-machine source provides adequate power reserve. The P/V generator is usually implemented in PV decoupling mode, where the V generator is exactly the same as the V generator of the PV-type grid-forming nonsynchronous-machine source. When the output power reference value P_s^* of the P generator in the outermost loop in Figure 4 is decoupled from the grid frequency, the nonsynchronous-machine source lacks inertia support and primary frequency regulation capabilities. When P_s^* is proportional to the derivative of the power grid frequency, the nonsynchronous-machine source has the inertia support capability. When P_s^* is related to the frequency deviation of the power grid, the nonsynchronous-machine source has the ability of primary frequency regulation.

When the nonsynchronous-machine source possesses both inertia support and primary frequency regulation capabilities, the active power reference value generated by the P generator is typically expressed as (18), where P_{s0} is the constant power component; f_0 is the rated frequency of the power grid; f is the actual frequency of the power grid; M_{non} is the equivalent inertial time constant of the nonsynchronous-machine source; and k_{non} is the proportional coefficient of the primary frequency regulation of the nonsynchronous-machine source.

$$P_s^* = P_{s0} + M_{non}\frac{\mathrm{d}f}{\mathrm{d}t} + k_{non}(f_0 - f) \tag{18}$$

For the PQ-type grid-following nonsynchronous-machine source in Figure 5, its inertia support and primary frequency regulation capabilities are determined by the outermost loop P/Q generator. Still, the premise is that the nonsynchronous-machine source provides adequate power reserve. The P/Q generator is usually implemented separately according to the PQ decoupling method, where the outermost P generator is the same as the PV-type grid-following nonsynchronous-machine source. When the PQ-type grid-following nonsynchronous-machine source has both inertia support and primary frequency regulation capabilities, the active power reference value generated by the P generator is also typically expressed as (18).

6.2. Definition and Calculation Method of the Inertia Support Strength of Nonsynchronous-Machine Sources

The direct manifestation of inertia is the RoCoF. Specifically, the initial RoCoF under a disturbance is exclusively associated with the inertia and the disturbance itself. Thus, the calculation of inertia can be transformed into the calculation of the initial RoCoF.

For a specific power system, there is a maximum limit for RoCoF [56], such as limiting the maximum RoCoF to 1 Hz/s, etc. The minimum inertia requirement is usually calculated from the maximum limit value of the RoCoF and the anticipated maximum active power disturbance. Different power grids have different standards regarding the maximum anticipated active power disturbance. For instance, the maximum active power disturbance specified by the European power grid is the loss of 3000 MW generation power [11], while the maximum active disturbance specified by the Chinese power grid is generally the bipolar blocking of a single maximum UHVDC transmission line [70,71].

In this paper, the Equivalent Inertia Lifting Factor (EILF) is utilized to characterize the inertia support strength of the nonsynchronous-machine source. The derivation process is as follows. Under the specified maximum active power disturbance, the initial RoCoF of a node in the grid is (19) [12,16].

$$\left.\frac{\mathrm{d}f_{node}}{\mathrm{d}t}\right|_{t=0} = k_{const}\frac{\Delta P_{max}}{H_{eq}} \tag{19}$$

where k_{const} is a constant related to the operation state of the system; P_{max} is the unbalanced power under the specified maximum active power disturbance; and H_{eq} is the equivalent inertial time constant of the system under the investigated operation state.

For the investigated operation state of the system, we define $\left.\frac{\mathrm{d}f_{\mathrm{node}}}{\mathrm{d}t}\right|_{t=0}^{0}$ to represent $\left.\frac{\mathrm{d}f_{\mathrm{node}}}{\mathrm{d}t}\right|_{t=0}$ when all nonsynchronous-machine sources adopt the controllers without inertial support abilities. The controllers without inertial support abilities can be realized by setting H and M_{non} to zero in Figure 10 and (18). Then we define $\left.\frac{\mathrm{d}f_{\mathrm{node}}}{\mathrm{d}t}\right|_{t=0}^{1}$ to represent $\left.\frac{\mathrm{d}f_{\mathrm{node}}}{\mathrm{d}t}\right|_{t=0}$ when all nonsynchronous-machine sources adopt the controllers with inertial support abilities. Then, the equivalent inertia lifting value contributed by the nonsynchronous-machine sources with the inertial support controllers is defined as the Equivalent Inertia Lifting Factor H_{amp}, as shown in (20).

$$H_{\mathrm{amp}} = \frac{H_{\mathrm{eq}}^{1}}{H_{\mathrm{eq}}^{0}} = \left.\frac{\mathrm{d}f}{\mathrm{d}t}\right|_{t=0}^{0} \Big/ \left.\frac{\mathrm{d}f}{\mathrm{d}t}\right|_{t=0}^{1} \tag{20}$$

In (20), H_{eq}^{0} represents the equivalent inertia time constant of the whole power system when all the nonsynchronous-machine sources are controlled without inertial support abilities. H_{eq}^{1} represents the equivalent inertia time constant of the whole power system when all the nonsynchronous-machine sources are controlled with inertial support abilities. Therefore, H_{amp} can represent the inertia support strength of the nonsynchronous-machine sources. According to (20), H_{amp} is suitable for digital simulation calculations, and the initial $\left.\frac{\mathrm{d}f_{\mathrm{node}}}{\mathrm{d}t}\right|_{t=0}$ of a disturbance can be obtained by numerical differentiation. In addition, the grid nodes for evaluating the inertia support strength should be chosen based on the actual situation of the grid, and multiple nodes can be chosen simultaneously. Generally, the power grid regions with an insufficient number of synchronous generators are chosen because their RoCoFs are usually the largest; that is, their inertia support strength is the weakest.

6.3. Definition and Calculation Method of the Primary Frequency Regulation Capability of Nonsynchronous-Machine Sources

The primary frequency regulation capability can be represented by the frequency deviation factor [2,72]. In the new type of power system, the frequency deviation factor β can be defined as (21).

$$\beta = \frac{1}{R_{\mathrm{gen}}} + D_{\mathrm{load}} + K_{\mathrm{non}} \tag{21}$$

where R_{gen} is the equivalent droop of all synchronous generator governors, where the unit is Hz/MW; K_{non} is the equivalent frequency regulation coefficient of all nonsynchronous-machine sources, where the unit is MW/Hz; D_{load} is the frequency regulation coefficient of the system active power load, and its unit is MW/Hz. The common unit of β is MW/0.1 Hz.

β represents the relationship between the active power disturbance ΔP and the steady-state frequency deviation Δf_{∞}, as shown in (22).

$$\Delta f_{\infty} = \frac{\Delta P}{\beta} \tag{22}$$

Imitating the definition of inertia support strength, the steady-state frequency deviation decreasing factor R_{deltf} is adopted to describe the primary frequency regulation capability of the nonsynchronous-machine sources in this paper. R_{deltf} is defined as (23).

$$R_{\mathrm{deltf}} = \frac{\Delta f_{\infty}^{1}}{\Delta f_{\infty}^{0}} = \frac{\beta^{0}}{\beta^{1}} \tag{23}$$

where Δf_{∞}^{0} and β^{0} are the steady-state frequency deviation and the frequency deviation factor when all the nonsynchronous-machine sources are controlled without primary frequency regulation abilities. Δf_{∞}^{1} and β^{1} are the steady-state frequency deviation and frequency deviation factors when all the nonsynchronous-machine sources are controlled

with primary frequency regulation abilities. Therefore, R_{deltf} can represent the primary frequency regulation capabilities of the nonsynchronous-machine sources. According to (23), R_{deltf} can be calculated easily using digital simulation. It is worth noting that the selected frequency monitoring point impacts both H_{amp} and R_{deltf} because the frequency of different nodes in the network varies during the transient process.

6.4. Simulation Validation

A modified IEEE 39-mode test system, as represented in Figure 15, is built to assess the efficacy of the suggested frequency support strength indices. The installed capacity of the synchronous generator sources is 7600 MW, while the installed capacity of the nonsynchronous-machine sources is 2072 MW. The average inertia of the synchronous generator sources is 4.55, and the rotational reserve rate is 10%. In Figure 15, the nonsynchronous-machine sources are connected to buses 4, 18, and 21 accordingly.
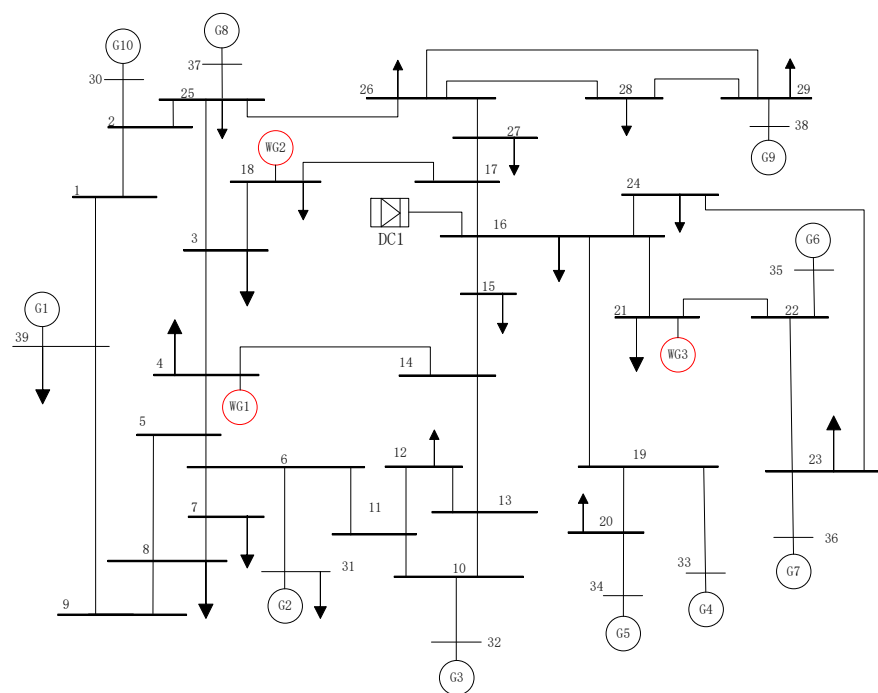
Figure 15. Modified IEEE 39-node test system.

The following two scenarios are considered to calculate the equivalent inertia lifting factor and the steady-state frequency deviation decreasing factor. Firstly, when all the nonsynchronous-machine sources adopt the constant active power control and the constant reactive power control, they have no frequency support abilities. The RoCoF and the steady-state frequency deviation can be obtained by the simulation. As shown in Figure 16, $\left.\frac{\mathrm{d}f_{\text{node}}}{\mathrm{d}t}\right|_{t=0}^{0} = 0.303 \, \text{Hz/s}$, and $\Delta f_{\infty}^{0} = -0.136 \, \text{Hz}$. Then, when all the nonsynchronous-machine sources adopt the PSL control and the constant reactive power control, they have both inertia support and primary frequency regulation. M_{non} of all the nonsynchronous-machine sources is set to 6.8, and k_{non} is set to 30. As shown in Figure 16, $\left.\frac{\mathrm{d}f_{\text{node}}}{\mathrm{d}t}\right|_{t=0}^{1} = 0.214 \, \text{Hz/s}$, and $\Delta f_{\infty}^{1} = -0.096 \, \text{Hz}$. Therefore, H_{amp} is 1.416, and R_{deltf} is 0.706.
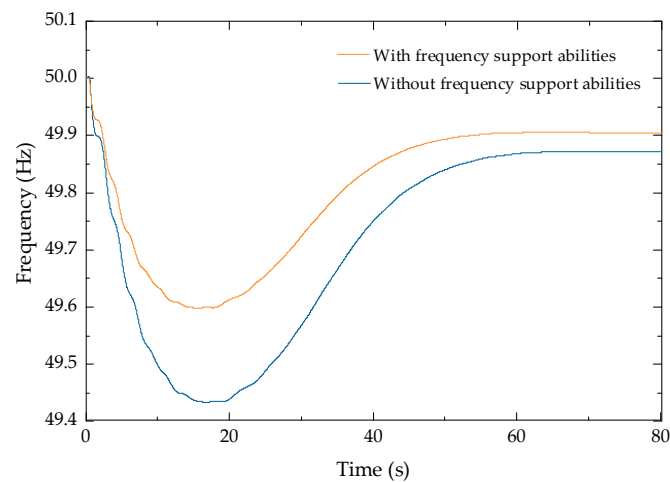
Figure 16. Frequency characteristic curves when all the nonsynchronous-machine sources are controlled with and without frequency support abilities, respectively.

7. Conclusions

The fundamental characteristic of the new type of power system is that the dominant sources have shifted from traditional synchronous generators to nonsynchronous-machine sources. Accordingly, the definitions and calculation methods of power grid strength must be revised. This paper has investigated these challenges, and the key conclusions are given below.

(1) Nonsynchronous-machine sources can be categorized into four types at the macro level: Vθ type grid-forming, PV-type grid-forming, PV-type grid-following, and PQ-type grid-following.

(2) The external characteristics of nonsynchronous-machine sources are closely related to their operating states. Once they reach the current saturation state, their control objectives cannot be realized.

(3) The classical SCR index can be defined by the Thevenin equivalent impedance of the power grid and the equivalent impedance of the connected device. This definition is more suitable for describing the effect of nonsynchronous-machine sources on the voltage support strength.

(4) The voltage stiffness index K_{vtg} presented in this paper reflects more comprehensive information than SCR since it considers the respective impedance angles of both the Thevenin equivalent impedance and the equivalent impedance of the connected device.

(5) The physical significance of the multiple DC infeed SCR is further clarified by the multi-port Thevenin equivalent circuit, where the essence is that when multiple nodes in the grid simultaneously connect loads, the voltage drop on each node is larger than when a single node connects a load alone.

(6) The inertia support capability of nonsynchronous-machine sources can be described by the equivalent inertia lifting factor, while the primary frequency regulation capability of nonsynchronous-machine sources can be described by the steady-state frequency deviation decreasing factor.

Conflicts of Interest: The authors declare no conflict of interest.

References

1. Anderson, P.; Fouad, A. *Power System Control and Stability*, 2nd ed.; IEEE Press: New York, NY, USA, 2003.
2. Kundur, P.S. *Power System Stability and Control*; McGraw-Hill: New York, NY, USA, 1994.
3. Machowski, J.; Blalek, J.; Bumby, J. *Power System Dynamics-Stability and Control*; John Wiley & Sons Ltd.: New York, NY, USA, 2008.
4. CIGRE Working Group 14.07; IEEE Working Group 15.05.05. *Guide for Planning DC Links Terminating at AC Locations Having Low Short-Circuit Capacities-Part I: AC/DC Interaction Phenomena*; CIGRE Brochure: Paris, France, 1992; p. 68.
5. CIGRE Working Group 14.07; IEEE Working Group 15.05.05. *Guide for Planning DC Links Terminating at AC Locations Having Low Short-Circuit Capacities-Part II: Planning Guidelines*; CIGRE Brochure: Paris, France, 1997; p. 115.
6. IEEE. *IEEE Guide for Planning DC Links Terminating at AC Locations Having Low Short-Circuit Capacities*; IEEE Std 1204-1997: New York, NY, USA, 1997.
7. Xin, H.; Dong, W.; Yuan, X.; Gan, D.; Wu, D. Generalized short circuit ratio for multi power electronic based devices infeed to power systems. *Proc. CSEE* **2016**, *36*, 6013–6027.
8. Sun, H.; Xu, S.; Xu, T.; Guo, Q.; He, J.; Zhao, B.; Zhu, Y. Definition and index of short circuit ratio for multiple renewable energy stations. *Proc. CSEE* **2021**, *41*, 497–505.
9. Sui, T.; Mo, Y.; Marelli, D.; Sun, X.-M.; Fu, M. The Vulnerability of Cyber-Physical System Under Stealthy Attacks. *IEEE Trans. Autom. Control* **2021**, *66*, 637–650. [CrossRef]
10. Sui, T.; Sun, S. The vulnerability of distributed state estimator under stealthy attacks. *Automatica* **2021**, *113*, 109869. [CrossRef]
11. ENTSO-E. *Frequency Stability Evaluation Criteria for the Synchronous Zone of Continental Europe*; ENTSO-E: Brussels, Belgium, 2016.
12. ENTSO-E. *Future System Inertia*; ENTSO-E: Brussels, Belgium, 2016.
13. ENTSO-E. *Parameters Related to Frequency Stability*; ENTSO-E: Brussels, Belgium, 2016.
14. ENTSO-E. *Limited Frequency Sensitive Mode*; ENTSO-E: Brussels, Belgium, 2018.
15. ENTSO-E. *Need for Synthetic Inertia (SI) for Frequency Regulation*; ENTSO-E: Brussels, Belgium, 2018.
16. ENTSO-E. *Inertia and Rate of Change of Frequency (RoCoF)*; ENTSO-E: Brussels, Belgium, 2020.
17. ENTSO-E. *Frequency Ranges*; ENTSO-E: Brussels, Belgium, 2021.
18. ENTSO-E. *System Defense Plan*; ENTSO-E: Brussels, Belgium, 2022.
19. Cao, X.; Stephen, B.; Abdulahadi, I.; Booth, C.D.; Burt, G.M. Switching Markov Gaussian models for dynamic power system inertia estimation. *IEEE Trans. Power Syst.* **2016**, *31*, 3394–3403. [CrossRef]
20. Tuttelberg, K.; Kilter, J.; Wilson, D.; Uhlen, K. Estimation of power system inertia from ambient wide area measurements. *IEEE Trans. Power Syst.* **2018**, *33*, 7249–7257. [CrossRef]
21. Milano, F.; Dörfler, F.; Hug, G.; Hill, D.J.; Verbič, G. Foundations and challenges of low-inertia systems (Invited Paper). In Proceedings of the 2018 Power Systems Computation Conference (PSCC), Dublin, Ireland, 11–15 June 2018; pp. 1–25.
22. Fernández-Guillamóna, A.; Gómez-Lázaro, E.; Muljadi, E.; Molina-García, Á. Power systems with high renewable energy sources: A review of inertia and frequency control strategies over time. *Renew. Sustain. Energy Rev.* **2019**, *115*, 109369. [CrossRef]
23. Xu, Z. Three Technical Challenges Faced by Power Systems in Transition. *Energies* **2022**, *15*, 4473. [CrossRef]
24. Ortjohann, E.; Arias, A.; Morton, D.; Mohd, A.; Hamsic, N.; Omari, O. Grid-forming three-phase inverters for unbalanced loads in hybrid power systems. In Proceedings of the 2006 IEEE 4th World Conference on Photovoltaic Energy Conversion, Waikoloa, HI, USA, 7–12 May 2006; pp. 2396–2399.
25. Ninad, N.; Lopes, L. Per-phase vector (dq) controlled three-phase grid-forming inverter for stand-alone systems. In Proceedings of the 2011 IEEE International Symposium on Industrial Electronics, Gdansk, Poland, 27–30 June 2011; pp. 1626–1631.
26. Pattabiraman, D.; Lasseter, R.; Jahns, T. Comparison of grid following and grid forming control for a high inverter penetration power system. In Proceedings of the 2018 IEEE Power & Energy Society General Meeting (PESGM), Portland, OR, USA, 5–10 August 2018; pp. 1–5.
27. Rosso, R.; Wang, X.; Liserre, M.; Lu, X.; Engelken, S. Grid-forming converters: Control approaches, grid-synchronization, and future trends–A review. *IEEE Open J. Ind. Appl.* **2021**, *2*, 93–109. [CrossRef]
28. ENTSO-E. *High Penetration of Power Electronic Interfaced Power Sources and the Potential Contribution of Grid Forming Converters*; ENTSO-E: Brussels, Belgium, 2021.
29. Shakerighadi, B.; Johansson, N.; Eriksson, R.; Mitra, P.; Bolzoni, A.; Clark, A.; Nee, H. An overview of stability challenges for power-electronic-dominated power systems: The grid-forming approach. *IET Gener. Transm. Distrib.* **2022**, 1–23. [CrossRef]
30. Khan, S.; Wang, M.; Su, W.; Liu, G.; Chaturvedi, S. Grid-forming converters for stability issues in future power grids. *Energies* **2022**, *15*, 4937. [CrossRef]
31. Musca, R.; Gonzalez-Longatt, F.; Gallego Sánchez, C. Power system oscillations with different prevalence of grid-following and grid-forming converters. *Energies* **2022**, *15*, 4273. [CrossRef]
32. Zhang, C.; Zhang, X. *PWM Rectifier and Its Control*; China Machine Press: Beijing, China, 2003.
33. Chen, H.; Xu, Z. Control design for VSC-HVDC supplying passive network. *Proc. CSEE* **2006**, *26*, 42–48.
34. Xu, Z.; Xiao, H.; Zhang, Z.; Xue, Y.; Liu, G.; Tang, G.; Xu, F.; Wang, S.; Tu, Q.; Guan, M.; et al. *Voltage Source Converter Based HVDC Power Transmission Systems*, 2nd ed.; China Machine Press: Beijing, China, 2017; pp. 106–112.

35. Femia, N.; Petrone, G.; Spagnuolo, G.; Vitelli, M. *Power Electronics and Control Techniques for Maximum Energy Harvesting in Photovoltaic Systems*; CRC Press: New York, NY, USA, 2012.
36. Blaabjerg, F.; Teodorescu, R.; Liserre, M.; Timbus, A.V. Overview of control and grid synchronization for distributed power generation systems. *IEEE Trans. Ind. Electron.* **2006**, *53*, 1398–1409. [CrossRef]
37. Zhou, J.; Ding, H.; Fan, S.; Zhang, Y.; Gole, A.M. Impact of short-circuit ratio and phase-locked-loop parameters on the small-signal behavior of a VSC-HVDC converter. *IEEE Trans. Power Deliv.* **2014**, *29*, 2287–2296. [CrossRef]
38. Luna, A.; Rocabert, J.; Candela, I.; Hermoso, J.R.; Teodorescu, R.; Blaabjerg, F.; Rodriguez, P. Grid voltage synchronization for distributed generation systems under grid fault conditions. *IEEE Trans. Ind. Appl.* **2015**, *51*, 3414–3425. [CrossRef]
39. Du, D.; Chen, X.; Wang, H. Parameter tuning of the PLL to consider the effect on power system small-signal angular stability. *IET Renew. Power Gener.* **2018**, *12*, 1–8. [CrossRef]
40. Hu, Q.; Fu, L.; Ma, F.; Ji, F. Large signal synchronizing instability of PLL-based VSC connected to weak AC grid. *IEEE Trans. Power Syst.* **2019**, *34*, 3220–3228. [CrossRef]
41. He, X.; Geng, H.; Ma, S. Transient stability analysis of grid-tied converters considering PLL's nonlinearity. *CPSS Trans. Power Electron. Appl.* **2019**, *4*, 40–49. [CrossRef]
42. Qiu, G.; Luo, X. *Electric Circuits*, 5th ed.; Higher Education Press: Beijing, China, 2006.
43. Anderson, P. *Analysis of Faulted Power Systems*; John Wiley & Sons, INC.: New York, NY, USA, 1995.
44. Guan, M.; Xu, Z. Direct voltage control of MMC-based VSC-HVDC system for passive networks. *Electr. Power Autom. Equip.* **2012**, *32*, 1–5.
45. Lu, X.; Wang, J.; Guerrero, J.; Zhao, D. Virtual-impedance-based fault current limiters for inverter dominated AC microgrids. *IEEE Trans. Smart Grid* **2018**, *9*, 1599–1612. [CrossRef]
46. Liu, H.; Wang, Y.; Liu, Y.; Peng, Y.; Li, M.; Lei, W. The LVRT strategy for VSG based on the quantitatively designed virtual impedance. *High Volt. Eng.* **2022**, *48*, 245–256.
47. Xu, Z.; Zhang, Z.; Xu, W. Research on application of LCC-MMC series hybrid HVDC topology for large scale clean energy base integration. *Power Capacit. React. Power Compens.* **2022**, *43*, 119–126.
48. Xu, Z. Characteristics of HVDC connected to weak AC systems Part I: HVDC transmission capability. *Power Syst. Technol.* **1997**, *21*, 12–16.
49. Xu, Z. The characteristics of HVDC systems to weak ac systems part II: Control modes and voltage stability. *Power Syst. Technol.* **1997**, *21*, 1–4.
50. Xu, Z. *Dynamic Performance Analysis of AC/DC Power Systems*; China Machine Press: Beijing, China, 2004.
51. CIGRE Working Group B4.62. *Connection of Wind Farms to Weak AC Networks*; CIGRE: Paris, France, 2016.
52. Australian Energy Market Operator. *SYSTEM Strength Impact Assessment Guidelines*; AEMO: Melbourne, Australia, 2018.
53. CIGRE Working Group B4.41. Systems with multiple DC infeed. *ELECTRA* **2007**, *15*, 14–18.
54. CIGRE Working Group B4.41. *Systems with Multiple DC Infeed*; CIGRE: Paris, France, 2008.
55. Zhang, H.; Du, Y. Enlarging of the Thevenin's theorem in two-pole network. *J. Binzhou Teach. Coll.* **1999**, *15*, 32–33.
56. ENTSO-E. *Rate of Change of Frequency (RoCoF) Withstand Capability*; ENTSO-E: Brussels, Belgium, 2018.
57. Sun, H.; Wang, B.; Li, W.; Yang, C.; Wei, W.; Zhao, B. Research on inertia system of frequency response for power system with high penetration electronics. *Proceeding CSEE* **2020**, *40*, 5179–5191.
58. Zhang, L.; Harnrfors, L.; Nee, H. Power-synchronization control of grid-connected voltage-source converters. *IEEE Trans. Power Syst.* **2010**, *25*, 809–820. [CrossRef]
59. Zhang, L.; Harnefors, L.; Nee, H. Interconnection of two very weak AC systems by VSC-HVDC links using power-synchronization control. *IEEE Trans. Power Syst.* **2011**, *26*, 344–355. [CrossRef]
60. Beck, H.; Hesse, R. Virtual synchronous machine. In Proceedings of the 2007 9th International Conference on Electrical Power Quality and Utilization, Barcelona, Spain, 9–11 October 2007; pp. 1–5.
61. Driesen, J.; Visscher, K. Virtual synchronous generators. In Proceedings of the 2008 IEEE Power and Energy Society General Meeting-Conversion and Delivery of Electrical Energy in the 21st Century, Pittsburgh, PA, USA, 20–24 July 2008; pp. 1323–1325.
62. Van, T.; Visscher, K.; Diaz, J.; Karapanos, V.; Woyte, A.; Albu, M.; Federenciuc, D. Virtual synchronous generator: An element of future grid. In Proceedings of the 2010 IEEE PES Innovative Smart Grid Technologies Conference Europe, Gothenburg, Sweden, 11–13 October 2010; pp. 1–7.
63. Zhong, Q.; Weiss, G. Synchronverters: Inverters that mimic synchronous generators. *IEEE Trans. Ind. Electron.* **2011**, *58*, 1259–1267. [CrossRef]
64. Zhong, Q.; Nguyen, P.; Ma, Z.; Sheng, W. Self-synchronized synchronverters: Inverters without a dedicated synchronization unit. *IEEE Trans. Power Electron.* **2014**, *29*, 617–630. [CrossRef]
65. Guan, M.; Pan, W.; Zhang, J.; Hao, Q.; Cheng, J.; Zheng, X. Synchronous generator emulation control strategy for voltage source converter (VSC) stations. *IEEE Trans. Power Syst.* **2015**, *30*, 3093–3101. [CrossRef]
66. Zhang, Z.; Xue, Y.; Xu, Z. Versatile static synchronous machine and its reference machine following control strategy. *IET Renew. Power Gener.* **2022**, *16*, 3184–3196. [CrossRef]
67. Wu, H.; Wang, X. Design-oriented transient stability analysis of grid-connected converters with power synchronization control. *IEEE Trans. Ind. Electron.* **2019**, *66*, 6473–6482. [CrossRef]

68. Taul, M.; Wang, X.; Davari, P.; Blaabjerg, F. An overview of assessment methods for synchronization stability of grid-connected converters under severe symmetrical grid faults. *IEEE Trans. Power Electron.* **2019**, *34*, 9655–9670. [CrossRef]

69. Wang, X.; Taul, M.; Wu, H.; Liao, Y.; Blaabjerg, F.; Harnefors, L. Grid-synchronization stability of converter-based resources—An overview. *IEEE Open J. Ind. Appl.* **2020**, *1*, 115–134. [CrossRef]

70. Xu, Z.; Dong, H. Three basic constraints for the reasonable size of synchronous power systems. *Int. J. Electr. Power Energy Syst.* **2017**, *90*, 76–86. [CrossRef]

71. Xu, Z.; Dong, H.; Song, P.; Cheng, B. Three Basic Constraints for Reasonable Size of Synchronous Grids. *Electr. Power Constr.* **2015**, *36*, 77–84.

72. Xu, Z.; Song, P.; Huang, H. Three macroscopic indices for describing the quality of AC/DC power grid structures. *IET Gener. Transm. Distrib.* **2016**, *10*, 175–182. [CrossRef]